brain sciences

MDPI

Opinion

Challenges and Perspectives of Mapping Locus Coeruleus Activity in the Rodent with High-Resolution fMRI

Xiaoqing Alice Zhou [1], Yuanyuan Jiang [1], Vitaly Napadow [1,2] and Xin Yu [1,*]

[1] Athinoula A. Martinos Center for Biomedical Imaging, Massachusetts General Hospital, Charlestown, MA 02129, USA
[2] Department of Physical Medicine and Rehabilitation, Spaulding Rehabilitation Hospital, Harvard Medical School, Charlestown, MA 02129, USA
* Correspondence: xyu9@mgh.harvard.edu

Abstract: The locus coeruleus (LC) is one of the most commonly studied brainstem nuclei when investigating brain–behavior associations. The LC serves as a major brainstem relay for both ascending bottom-up and descending top-down projections. Specifically, noradrenergic (NA) LC neurons not only connect globally to higher-order subcortical nuclei and cortex to mediate arousal and attention but also directly project to other brainstem nuclei and to the spinal cord to control autonomic function. Despite the extensive investigation of LC function using electrophysiological recordings and cellular/molecular imaging for both cognitive research and the contribution of LC to different pathological states, the role of neuroimaging to investigate LC function has been restricted. For instance, it remains challenging to identify LC-specific activation with functional MRI (fMRI) in animal models, due to the small size of this nucleus. Here, we discuss the complexity of fMRI applications toward LC activity mapping in mouse brains by highlighting the technological challenges. Further, we introduce a single-vessel fMRI mapping approach to elucidate the vascular specificity of high-resolution fMRI signals coupled to LC activation in the mouse brainstem.

Keywords: locus coeruleus; fMRI; rodent brain; brainstem; single-vessel fMRI

Citation: Zhou, X.A.; Jiang, Y.; Napadow, V.; Yu, X. Challenges and Perspectives of Mapping Locus Coeruleus Activity in the Rodent with High-Resolution fMRI. *Brain Sci.* **2022**, *12*, 1085. https://doi.org/10.3390/brainsci12081085

Academic Editor: Oxana Eschenko

Received: 26 July 2022
Accepted: 12 August 2022
Published: 16 August 2022

The locus coeruleus (LC) is one of the most commonly investigated brainstem nuclei to explore brain–behavior associations [1–3]. Studies of LC noradrenergic (NA) pathway-mediated arousal can be traced back half a century [4], originating with investigations of the LC contribution to rapid eye movement (REM) sleep [5,6]. Although LC is a relatively small nucleus, it includes condensed NA neurons with broad projections throughout the central nervous system [7,8]. Such cellular specificity allows for effective stimulation with optogenetic or chemogenetic tools by introducing optical fibers or local microinjection of DREADD agonists [9,10] in rodent models. However, since LC is located deep within the dorsal pontine area of the brainstem, this nucleus remains difficult to image with conventional optical imaging methods. In vivo electrophysiological recording is typically used to measure LC-specific NA neuronal activity based on unique firing patterns, which can guide the precise localization of electrode placement [11]. However, NA influence is widespread in the brain, and the cortical and subcortical neuromodulatory effects of LC firing have been difficult to assess. To bridge LC-specific NA activation and its brain-wide neuromodulatory effects, functional MRI (fMRI) has been applied to explore LC activity and influence on other brain regions for both animal and human brains [12,13]. In this review, we mainly focus on elucidating the challenges of applying fMRI methods to precisely target LC neuronal activity in the rodent brain.

Can fMRI accurately assess LC activity in the mouse brain with sufficient resolution? The mouse LC has a cross-sectional diameter of ~300 µm and a slightly longer dimension along the rostral–causal brainstem axis [14]. Conventional application of fMRI has used a two-dimensional (2D) echo-planar imaging (EPI) pulse sequence approach. Typical 2D

EPI-fMRI imaging of the mouse brain can be performed with an in-plane resolution of 200 × 200 µm and 500 µm slice thickness, e.g., awake mouse fMRI using a 14 T scanner [15]. Hence, given this spatial resolution, the mouse LC would be typically comprised of fewer than four voxels and notable partial volume effects of these voxels due to contributions from adjacent nuclei. Moreover, for group analysis, cross-subject coregistration methods contribute additional smoothening effects for the signal from the LC, further reducing LC anatomical specificity of the fMRI signal. It should be noted that the resting-state functional connectivity mapping related to the LC-NE pathway mainly encompasses major whole-brain resting-state networks [9,10] and may not reflect LC-specific low-frequency signal fluctuations, due to a lack of sufficient spatial resolution with the conventional fMRI methods noted above.

To improve LC spatial specificity in fMRI, a better appreciation of the causes of limited spatial resolution of fMRI is needed. The first issue includes limits of the signal-to-noise ratio (SNR) for task-related and resting-state fMRI using conventional mapping methods, e.g., echo-planar imaging (EPI), to acquire time-series datasets with a 1 or 2 s sample rate, i.e., the time of repetition (TR). Smaller voxel size is associated with a lower SNR due to a reduced number of water protons in the voxel. The second issue is the strength of the MRI gradient and its slew rate (i.e., how fast to approach the peak amplitude of the gradient) needed to yield high spatial resolution fMRI across the mouse brain at a selected time of echo (TE). TE is the free induction decay (FID) time of water spins following radiofrequency (RF) pulses to acquire a T2*-weighted signal, which represents the change in field homogeneity due to neuronal activity-coupled hemodynamic responses, e.g., the blood oxygen level-dependent (BOLD) fMRI signal [16–19]. The neuronal activity-coupled T2* contrast changes vary at different TE, which can be influenced by the intrinsic susceptibility of the samples (blood vs. parenchyma voxels), the field strength-dependent T2* of brain tissue, and the echo-train duration during acquisition [20–23]. To optimize the T2* contrast for a small nucleus like the LC, we need to optimize the TE and echo acquisition, and improved gradient performance is critical for such high spatial resolution data acquisition.

To solve these technological challenges, ultrahigh-field preclinical MR scanners (>11.7 Tesla) and multiarray cryoprobe [24] or implanted RF coils [25] have been applied to boost the SNR, while high-performance gradients (e.g., 1 T/m gradient strength) can be coupled with an ultrahigh-field scanner to enable high spatial resolution mapping [26,27]. Moreover, several advanced denoising algorithms [28] have been developed to remove background noise and further improve the SNR of high-resolution fMRI images [29]. Ultimately, using a 14 Tesla MRI scanner, the spatial resolution of mouse brain fMRI can approach 100 um isotropic [30], a substantial improvement in spatial resolution, making it possible to record fMRI signals from dozens of LC voxels. Additionally, it should be noted that the LC in human brains is much larger than in mice. The human LC is ~14.5 mm long and 2–2.5 mm in cross-sectional diameter for this nucleus located 1–1.5 mm away from the floor of the fourth ventricle [31], a high source of noise due to CSF fluctuations. For human MRI, the ultrahigh field is typically 7 T and above, with fMRI data from 10.5 Tesla scanners approaching 400 um isotropic resolution, allowing for better localization of LC [29,32]. Such promising advances in high-resolution human fMRI could lead to significant advances in human LC research.

What is the spatial specificity of fMRI to map LC activation? It has been well understood that fMRI signals, e.g., typical BOLD [16] or cerebral blood volume (CBV; [33] contrasts, originate from blood-based contrast mechanisms and are sensitive to blood vessel density and physiology. In contrast to human fMRI using 3 T or 7 T scanners, rodent fMRI is typically performed using specialized preclinical MRI scanners operating at field strengths above 9.4 T. Using ultrahigh-field strength, e.g., 14 T, to improve the spatial resolution of fMRI to 100 × 100 um in-plane, Yu et al. recently reported that individual penetrating venules dominated BOLD signals because of the high oxygen:hemoglobin (Hb) ratio changes in venous blood, while arterioles dominate CBV signals due to the smooth muscle

cell-controlled arterial dilation in both deep cortex [26,34] (Figure 1) and hippocampus [35]. These microscale vessels have 20–70 micron diameter and are separated by 300–400 microns, connecting large draining veins or feeding arteries to higher-order vascular branches toward capillary beds [36,37].

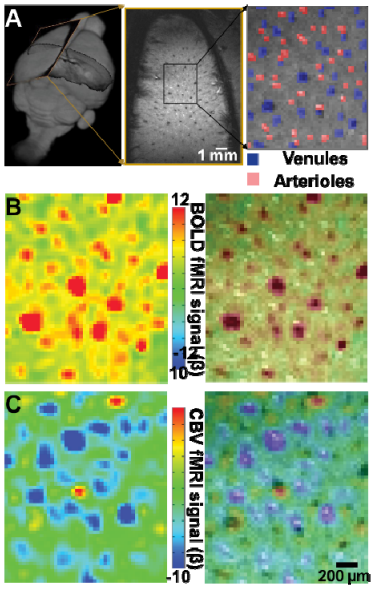

Figure 1. Vessel-specific BOLD and CBV signals with single-vessel fMRI. (**A**). 2D multigradient-echo (MGE) slice is acquired across the deep-layer cortex to identify penetrating arterioles (red) and venules (blue). (**B**). The evoked BOLD fMRI signal of the forepaw somatosensory cortex (FP-S1) is located at the penetrating venules. (**C**). The evoked CBV fMRI signal of FP-S1 is located at the penetrating arterioles. Adapted from Yu et al. 2016.

The LC is located in the superior dorsal pontine area, near the fourth ventricle of mouse brains. High-resolution micro-CT has been used to identify the microvasculature of the mouse brainstem, showing the densely packed choroid plexus in the fourth ventricle and penetrating vessels supplying blood to the dorsal–rostral pontine area close to the LC [38] (Figure 2). While there has not been a report of brainstem functional mapping with single-vessel fMRI, it is highly plausible to detect activation-coupled peak hemodynamic responses located at specific penetrating vessels supplying blood to the LC, which could also spread to the choroid plexus. The fMRI signal from LC parenchymal voxels would show much less contrast-to-noise ratio (CNR) difference compared to surrounding vessel voxels. This hypothesized technique would extend LC-specific fMRI from a nuclei-specific approach to a vessel-specific spatial pattern approach, consistent with the vascular origin of fMRI.

To better differentiate the vascular contribution to LC spatial specificity with high-resolution fMRI, it is important to specify intravascular versus extravascular effects on T2*-weighted signals to a given voxel [39]. The vascular volume fraction of brain tissue is usually less than 2–5% [40–42]. When the voxel size (e.g., 1 mm isotropic) is significantly larger than the vessel size, the intravascular signal contribution to the overall T2* signal in the voxel is small, given its volume fraction. This vascular effect would be more negligible at high magnetic field strength because of the faster T2* decay of venous blood, despite its higher oxy/deoxygenation ratio changes compared to other compartments in the voxel. Also, the extravascular influence of blood can be further reduced by a spin-echo sequence, which introduces a 180-degree radiofrequency pulse to resume additional dephasing during the free induction decay caused by the static field distortion of larger vessels [43–45]. It should be noted that fMRI signals of large voxels weigh more on capillary beds, which are closer to the source of parenchymal neuronal activation. In contrast, when the voxel size is smaller (e.g., 100 um isotropic), the penetrating vessel, which is tens of microns in

diameter, presents a much higher volume fraction, and its vascular contribution to the T2*-weighed fMRI signal would not be negligible, but may even dominate the BOLD or CBV effects, as previously reported by Yu et al. [20], Thus, when the spatial resolution of fMRI is further improved, a more refined vessel-specific fMRI signal may be evident across brainstem functional nuclei, including LC.

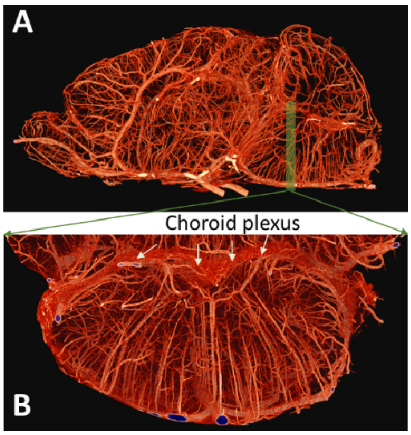

Figure 2. High-resolution micro-CT-based cerebrovascular mapping in the mouse brainstem. (**A**) Sagittal view and (**B**) coronal view of vascular structure supplying the superior dorsal pontine area), adapted from Hlushchuk et al. 2020.

What does the future of high-resolution LC fMRI promise? While the role of neuroimaging to investigate LC function has been restricted, mainly due to technical challenges in identifying LC-specific activation with fMRI, these challenges may be overcome to yield a more robust recording of fMRI signals from the LC. The application of LC-specific high-resolution fMRI mapping could lead to multiple novel insights relevant to LC-NA mediated neuromodulatory function. First, most fMRI studies use general linear models (e.g., linear regression) for analysis of the fMRI signal, incorporating a canonical hemodynamic response function (HRF). This HRF relies on the underlying neurovascular coupling features of local brain regions, which are based on the cellular components and vascular structure within the parenchyma. Different HRFs across subcortical nuclei have been reported, for instance for hippocampal activity in monkey brains [46]. In fact, the estimation of a regionally specific HRF relies not only on voxel location but also on voxel size. High-resolution fMRI could provide a more precise estimation of the vessel-specific HRF located at the LC and distinguish it from spreading responses associated with the choroid plexus of the fourth ventricle. This LC-specific vascular hemodynamic mapping could enable the comparison of neurovascular coupling effects and HRFs between the LC and other cortical and subcortical structures. Also, high-resolution fMRI may allow for the ability to distinguish LC-coupled vascular responses from activation of adjacent functional nuclei, e.g., the parabrachial (PB) nucleus [47,48]. Although similar brainstem-penetrating vessels may supply blood to both nuclei, the vessel-specific dynamic patterns could be characterized if LC- or PB-specific neural circuit activity is manipulated with optogenetic or chemogenetic tools. Moreover, high-resolution fMRI will provide a unique neuroimaging platform to map cross-scale vasodynamics mediated through the LC-NA pathway. Either NA-mediated vasoconstriction or intrinsic dynamic vasomotor changes could be directly mapped with a single-vessel fMRI technique, in combination with LC-specific vascular dynamic changes.

As one of the most commonly studied brainstem nuclei, the LC is critical for a wide array of brain–behavior associations. Given its tiny size and unique spatial localization in the brainstem, how to precisely locate LC function in the context of cross-scale brain dynamic mapping is an ongoing challenge. High-resolution awake mouse fMRI, in particular with ultrahigh field strength, in combination with other optogenetic or chemogenetic techniques will yield insights into deciphering the LC-NE circuitry contribution to more

complex arousal and attention regulation. Meanwhile, other emerging imaging techniques, e.g., functional ultrasound (fUS)and optoacoustic (fOA) imaging, have been developed for large-scale high spatiotemporal resolution rodent brain imaging [49–54]. In particular, fUS is also adept at detecting vessel-specific vasodynamic changes, which mimic single-vessel fMRI results when sufficient SNR is present in deep brain regions, e.g., the LC of awake mice. It should also be noted that to achieve optimal signal transmission for fOA or fUS, rodents need to have either a thin skull or a large craniotomy needs to be performed. However, both fOA and fUS are characterized by more efficient spectral transmission through brain tissue than conventional optical imaging methods. In summary, the LC is a critically important brainstem nucleus, and newer imaging modalities are beginning to show promise for capturing functional activity from the LC for many research applications.

Author Contributions: Conceptualization, X.A.Z. and X.Y.; validation, V.N. and X.Y.; investigation, X.A.Z. and X.Y.; resources, X.A.Z., Y.J. and X.Y.; writing—original draft preparation, X.A.Z. and X.Y.; writing—review and editing, X.A.Z., Y.J., V.N. and X.Y.; visualization, X.A.Z., Y.J., V.N. and X.Y.; supervision, V.N. and X.Y.; project administration, V.N. and X.Y.; funding acquisition, X.Y. All authors have read and agreed to the published version of the manuscript.

Funding: This research was funded by NIH Brain Initiative funding (RF1NS113278, R01 MH111438, R01NS122904), NSF grant 2123971, and the S10 instrument grant (S10 MH124733–01) to Martinos Center.

Conflicts of Interest: The authors declare no conflict of interest.

References

1. Sara, S.J. The locus coeruleus and noradrenergic modulation of cognition. *Nat. Rev. Neurosci.* **2009**, *10*, 211–223. [CrossRef] [PubMed]
2. Breton-Provencher, V.; Drummond, G.T.; Sur, M. Locus Coeruleus Norepinephrine in Learned Behavior: Anatomical Modularity and Spatiotemporal Integration in Targets. *Front. Neural Circuits* **2021**, *15*, 46. [CrossRef] [PubMed]
3. Poe, G.R.; Foote, S.; Eschenko, O.; Johansen, J.P.; Bouret, S.; Aston-Jones, G.; Harley, C.W.; Manahan-Vaughan, D.; Weinshenker, D.; Valentino, R.; et al. Locus coeruleus: A new look at the blue spot. *Nat. Rev. Neurosci.* **2020**, *21*, 644–659. [CrossRef] [PubMed]
4. Roussel, B.; Buguet, A.; Bobillier, P.; Jouvet, M. Locus ceruleus, paradoxal sleep, and cerebral noradrena-line. *CR Seances Soc. Biol. Fil.* **1967**, *161*, 2537–2541.
5. Aston-Jones, G.; Shipley, M.; Chouvet, G.; Ennis, M.; Van Bockstaele, E.; Pieribone, V.; Shiekhattar, R.; Akaoka, H.; Drolet, G.; Astier, B. Afferent regulation of locus coeruleus neurons: Anatomy, physiology and pharmacology. *Prog. Brain Res.* **1991**, *88*, 47–75.
6. Mallick, B.N.; Pandi-Perumal, S.; Mccarley, R.W.; Morrison, A.R. *Rapid Eye Movement Sleep: Regulation and Function*; Cambridge University Press: Cambridge, UK, 2011.
7. Aston-Jones, G.; Chiang, C.; Alexinsky, T. Discharge of noradrenergic locus coeruleus neurons in behaving rats and monkeys suggests a role in vigilance. *Prog. Brain Res.* **1991**, *88*, 501–520. [CrossRef]
8. Li, Y.; Hickey, L.; Perrins, R.; Werlen, E.; Patel, A.A.; Hirschberg, S.; Jones, M.; Salinas, S.; Kremer, E.; Pickering, A.E. Retrograde optogenetic characterization of the pontospinal module of the locus coeruleus with a canine adenoviral vector. *Brain Res.* **2016**, *1641*, 274–290. [CrossRef]
9. Zerbi, V.; Floriou-Servou, A.; Markicevic, M.; Vermeiren, Y.; Sturman, O.; Privitera, M.; Von Ziegler, L.; Ferrari, K.D.; Weber, B.; De Deyn, P.P.; et al. Rapid Reconfiguration of the Functional Connectome after Chemogenetic Locus Coeruleus Activation. *Neuron* **2019**, *103*, 702–718. [CrossRef]
10. Oyarzabal, E.A.; Hsu, L.-M.; Das, M.; Harry Chao, T.-H.; Zhou, J.; Song, S.; Zhang, W.; Smith, K.G.; Scio-Lino, N.R.; Evsyukova, I.Y.; et al. Chemogenetic Stimulation of Tonic Locus Coeruleus Activity Strengthens the Default Mode Network. *bioRxiv* **2021**. [CrossRef]
11. Eschenko, O.; Sara, S.J. Learning-dependent, transient increase of activity in noradrenergic neurons of locus coeruleus during slow wave sleep in the rat: Brain stem-cortex interplay for memory consolidation? *Cereb. Cortex* **2008**, *18*, 2596–2603. [CrossRef]
12. Liu, K.Y.; Marijatta, F.; Hämmerer, D.; Acosta-Cabronero, J.; Düzel, E.; Howard, R.J. Magnetic resonance imaging of the human locus coeruleus: A systematic review. *Neurosci. Biobehav. Rev.* **2017**, *83*, 325–355. [CrossRef]
13. Kelberman, M.; Keilholz, S.; Weinshenker, D. What's That (Blue) Spot on my MRI? Multimodal Neuroim-aging of the Locus Coeruleus in Neurodegenerative Disease. *Front. Neurosci.* **2020**, *14*, 583421. [CrossRef]
14. Schmidt, K.; Bari, B.; Ralle, M.; Washington-Hughes, C.; Muchenditsi, A.; Maxey, E.; Lutsenko, S. Localization of the Locus Coeruleus in the Mouse Brain. *J. Vis. Exp.* **2019**, *145*, e58652. [CrossRef]
15. Zeng, H.; Jiang, Y.; Beer-Hammer, S.; Yu, X. Awake Mouse fMRI and Pupillary Recordings in the Ultra-High Magnetic Field. *Front. Neurosci.* **2022**, *16*, 1028. [CrossRef]

16. Ogawa, S.; Lee, T.M.; Kay, A.R.; Tank, D.W. Brain magnetic resonance imaging with contrast dependent on blood oxygenation. *Proc. Natl. Acad. Sci. USA* **1990**, *87*, 9868–9872. [CrossRef]
17. Kwong, K.K.; Belliveau, J.W.; Chesler, D.A.; Goldberg, I.E.; Weisskoff, R.M.; Poncelet, B.P.; Kennedy, D.N.; Hoppel, B.E.; Cohen, M.S.; Turner, R.; et al. Dynamic magnetic resonance imaging of human brain activity during primary sensory stimulation. *Proc. Natl. Acad. Sci. USA* **1992**, *89*, 5675–5679. [CrossRef]
18. Ogawa, S.; Tank, D.W.; Menon, R.; Ellermann, J.M.; Kim, S.G.; Merkle, H.; Ugurbil, K. Intrinsic signal changes accompanying sensory stimulation: Functional brain mapping with magnetic resonance imaging. *Proc. Natl. Acad. Sci. USA* **1992**, *89*, 5951–5955. [CrossRef]
19. Bandettini, P.A.; Wong, E.C.; Hinks, R.S.; Tikofsky, R.S.; Hyde, J.S. Time course EPI of human brain function during task activation. *Magn. Reson. Med.* **1992**, *25*, 390–397. [CrossRef]
20. Yu, X.; Glen, D.; Wang, S.; Dodd, S.; Hirano, Y.; Saad, Z.; Reynolds, R.; Silva, A.C.; Koretsky, A.P. Direct imaging of macrovascular and microvascular contributions to BOLD fMRI in layers IV–V of the rat whisker–barrel cortex. *NeuroImage* **2012**, *59*, 1451–1460. [CrossRef]
21. Gati, J.S.; Menon, R.S.; Ugurbil, K.; Rutt, B.K. Experimental determination of the BOLD field strength de-pendence in vessels and tissue. *Magn. Reson. Med.* **1997**, *38*, 296–302. [CrossRef]
22. Donahue, M.J.; Hoogduin, H.; Smith, S.; Siero, J.; Chappell, M.; Petridou, N.; Jezzard, P.; Luijten, P.R.; Hendrikse, J. Spontaneous blood oxygenation level-dependent fMRI signal is modulated by behavioral state and correlates with evoked response in sensorimotor cortex: A 7.0-T fMRI study. *Hum. Brain Mapp.* **2012**, *33*, 511–522. [CrossRef]
23. Fera, F.; Yongbi, M.N.; Van Gelderen, P.; Frank, J.A.; Mattay, V.S.; Duyn, J.H. EPI-BOLD fMRI of human motor cortex at 1.5 T and 3.0 T: Sensitivity dependence on echo time and acquisition bandwidth. *J. Magn. Reson. Imaging* **2004**, *19*, 19–26. [CrossRef]
24. Baltes, C.; Radzwill, N.; Bosshard, S.; Marek, D.; Rudin, M. Micro MRI of the mouse brain using a novel 400 MHz cryogenic quadrature RF probe. *NMR Biomed.* **2009**, *22*, 834–842. [CrossRef]
25. Chen, Y.; Wang, Q.; Choi, S.; Zeng, H.; Takahashi, K.; Qian, C.; Yu, X. Focal fMRI signal enhancement with implantable inductively coupled detectors. *NeuroImage* **2022**, *247*, 118793. [CrossRef]
26. Yu, X.; He, Y.; Wang, M.; Merkle, H.; Dodd, S.J.; Silva, A.C.; Koretsky, A. Sensory and optogenetically driven single-vessel fMRI. *Nat. Chem. Biol.* **2016**, *13*, 337–340. [CrossRef]
27. Yu, X.; Qian, C.; Chen, D.-Y.; Dodd, S.J.; Koretsky, A.P. Deciphering laminar-specific neural inputs with line-scanning fMRI. *Nat. Methods* **2014**, *11*, 55–58. [CrossRef]
28. Veraart, J.; Novikov, D.S.; Christiaens, D.; Ades-Aron, B.; Sijbers, J.; Fieremans, E. Denoising of diffusion MRI using random matrix theory. *NeuroImage* **2016**, *142*, 394–406. [CrossRef]
29. Zhu, W.; Ma, X.; Zhu, X.-H.; Ugurbil, K.; Chen, W.; Wu, X. Denoise Functional Magnetic Resonance Imaging with Random Matrix Theory Based Principal Component Analysis. *IEEE Trans. Biomed. Eng.* **2022**, 1. [CrossRef]
30. Hike, D.C.; Liu, X.; Xie, Z.; Choi, S.; Jiang, Y.; Yu, X. Implanted RF coils enable 100um isotropic resolution EPI-fMRI images at ultra-high preclinical MRI scanner. *Proc. Soc. Neurosci.* **2022**.
31. Fernandes, P.; Regala, J.; Correia, F.; Gonçalves-Ferreira, A.J. The human locus coeruleus 3-D stere-otactic anatomy. *Surg. Radiol. Anat.* **2012**, *34*, 879–885. [CrossRef]
32. Vizioli, L.; Moeller, S.; Grant, A.; Tavaf, N.; Dowdle, L.; Sadeghi-Tarakameh, A.; Eryaman, Y.; Radder, J.; Lagore, R.; Van De Moortele, P.; et al. Ultra-High Resolution Human Functional Imaging Using 10.5 Tesla. In Proceedings of the High Field ISMRM Workshop, Champalimaud Foundation, Lisbon, Portugal, 19–22 March 2022.
33. Belliveau, J.W.; Kennedy, D.N.; McKinstry, R.C.; Buchbinder, B.R.; Weisskoff, R.M.; Cohen, M.S.; Vevea, J.M.; Brady, T.J.; Rosen, B.R. Functional Mapping of the Human Visual Cortex by Magnetic Resonance Imaging. *Science* **1991**, *254*, 716–719. [CrossRef] [PubMed]
34. He, Y.; Wang, M.; Chen, X.; Pohmann, R.; Polimeni, J.; Scheffler, K.; Rosen, B.R.; Kleinfeld, D.; Yu, X. Ultra-Slow Single-Vessel BOLD and CBV-Based fMRI Spatiotemporal Dynamics and Their Correlation with Neuronal Intracellular Calcium Signals. *Neuron* **2018**, *97*, 925–939. [CrossRef] [PubMed]
35. Chen, X.; Jiang, Y.; Choi, S.; Pohmann, R.; Scheffler, K.; Kleinfeld, D.; Yu, X. Assessment of single-vessel cerebral blood velocity by phase contrast fMRI. *PLoS Biol.* **2021**, *19*, e3000923. [CrossRef] [PubMed]
36. Stefanovic, B.; Hutchinson, E.; Yakovleva, V.; Schram, V.; Russell, J.T.; Belluscio, L.; Koretsky, A.; Silva, A.C. Functional Reactivity of Cerebral Capillaries. *J. Cereb. Blood Flow Metab.* **2008**, *28*, 961–972. [CrossRef]
37. Hirsch, S.; Reichold, J.; Schneider, M.; Szekely, G.; Weber, B. Topology and hemodynamics of the cortical cerebrovascular system. *J. Cereb. Blood Flow Metab.* **2012**, *32*, 952–967. [CrossRef]
38. Hlushchuk, R.; Haberthür, D.; Soukup, P.; Barré, S.F.; Khoma, O.-Z.; Schittny, J.; Haghayegh Jahromi, N.; Bouchet, A.; Engelhardt, B.; Djonov, V. Innovative high-resolution microCT imaging of animal brain vasculature. *Brain Struct. Funct.* **2020**, *225*, 2885–2895. [CrossRef]
39. Uludag, K.; Müller-Bierl, B.; Uğurbil, K. An integrative model for neuronal activity-induced signal changes for gradient and spin echo functional imaging. *NeuroImage* **2009**, *48*, 150–165. [CrossRef]
40. Weber, B.; Keller, A.L.; Reichold, J.; Logothetis, N.K. The microvascular system of the striate and ex-trastriate visual cortex of the macaque. *Cereb. Cortex* **2008**, *18*, 2318–2330. [CrossRef]

41. Leenders, K.L.; Perani, D.; Lammertsma, A.; Heather, J.D.; Buckingham, P.; Healy, M.J.R.; Gibbs, J.M.; Wise, R.J.S.; Hatazawa, J.; Herold, S.; et al. Cerebral Blood Flow, Blood Volume and Oxygen Utilization. Normal Values and Effect of Age. *Brain* **1990**, *113*, 27–47. [CrossRef]
42. Blinder, P.; Tsai, P.S.; Kaufhold, J.; Knutsen, P.M.; Suhl, H.; Kleinfeld, D. The cortical angiome: An interconnected vascular network with noncolumnar patterns of blood flow. *Nat. Neurosci.* **2013**, *16*, 889–897. [CrossRef]
43. Tanner, J.E.; Stejskal, E.O. Restricted Self-Diffusion of Protons in Colloidal Systems by the Pulsed-Gradient, Spin-Echo Method. *J. Chem. Phys.* **1968**, *49*, 1768–1777. [CrossRef]
44. Levitt, M.H.; Freeman, R. NMR population inversion using a composite pulse. *J. Magn. Reson.* **1979**, *33*, 473–476. [CrossRef]
45. Yacoub, E.; Duong, T.Q.; Van de Moortele, P.-F.; Lindquist, M.; Adriany, G.; Kim, S.-G.; Ugurbil, K.; Hu, X. Spin-echo fMRI in humans using high spatial resolutions and high magnetic fields. *Magn. Reson. Med.* **2003**, *49*, 655–664. [CrossRef]
46. Logothetis, N.K.; Eschenko, O.; Murayama, Y.; Augath, M.; Steudel, T.; Evrard, H.C.; Besserve, M.; Oeltermann, A. Hippocampal–cortical interaction during periods of subcortical silence. *Nature* **2012**, *491*, 547–553. [CrossRef]
47. Tsurugizawa, T.; Tamada, K.; Ono, N.; Karakawa, S.; Kodama, Y.; Debacker, C.; Hata, J.; Okano, H.; Kitamura, A.; Zalesky, A.; et al. Awake functional MRI detects neural circuit dysfunction in a mouse model of autism. *Sci. Adv.* **2020**, *6*, eaav4520. [CrossRef]
48. Henderson, L.A.; Macey, P.M.; Richard, C.A.; Runquist, M.L.; Harper, R.M. Functional magnetic resonance imaging during hypotension in the developing animal. *J. Appl. Physiol.* **2004**, *97*, 2248–2257. [CrossRef]
49. Boido, D.; Rungta, R.L.; Osmanski, B.-F.; Roche, M.; Tsurugizawa, T.; Le Bihan, D.; Ciobanu, L.; Charpak, S. Mesoscopic and microscopic imaging of sensory responses in the same animal. *Nat. Commun.* **2019**, *10*, 1110. [CrossRef]
50. Deffieux, T.; Demene, C.; Pernot, M.; Tanter, M. Functional ultrasound neuroimaging: A review of the pre-clinical and clinical state of the art. *Curr. Opin. Neurobiol.* **2018**, *50*, 128–135. [CrossRef]
51. Macé, E.; Montaldo, G.; Cohen, I.; Baulac, M.; Fink, M.; Tanter, M. Functional ultrasound imaging of the brain. *Nat. Methods* **2011**, *8*, 662–664. [CrossRef]
52. Liao, L.-D.; Lin, C.-T.; Shih, Y.-Y.I.; Duong, T.Q.; Lai, H.-Y.; Wang, P.-H.; Wu, R.; Tsang, S.; Chang, J.-Y.; Li, M.-L.; et al. Transcranial Imaging of Functional Cerebral Hemodynamic Changes in Single Blood Vessels using *in vivo* Photoacoustic Microscopy. *J. Cereb. Blood Flow Metab.* **2012**, *32*, 938–951. [CrossRef]
53. Yao, J.; Xia, J.; Wang, L.V. Multiscale Functional and Molecular Photoacoustic Tomography. *Ultrason. Imaging* **2016**, *38*, 44–62. [CrossRef]
54. Gottschalk, S.; Fehm, T.F.; Deán-Ben, X.L.; Tsytsarev, V.; Razansky, D. Correlation between volumetric oxygenation responses and electrophysiology identifies deep thalamocortical activity during epileptic seizures. *Neurophotonics* **2017**, *4*, 11007. [CrossRef]